Vapor-Assisted Remodeling of Thin Gold Films

Yuan Luo,[†] James Ruff,[†] Robert Ray,[†] Yunlong Gu,[‡] Harry J. Ploehn,[‡] and Walter A. Scrivens*,[†]

Departments of Chemistry & Biochemistry and of Chemical Engineering and USC Nanocenter, University of South Carolina, Columbia, South Carolina 29208

Received May 27, 2005. Revised Manuscript Received July 26, 2005

In this paper we present the results of a systematic study of the remodeling of ultrathin (<20 nm) gold films by exposure to condensable vapors of volatile solvents. The starting gold films, deposited on glass, consist of closely packed gold nanoparticles with controlled nominal thickness. Heating to relatively low temperature (60−120 °C) and exposure to condensable vapor carried by flowing N_2 gas lead to remodeling of the films' morphology. Electron and atomic force microscopy images show that the gold nanoparticles coalesce and form islands, interconnected networks, or holey continuous films, depending on the exposure time and the initial film thickness. Associated changes in the UV−vis spectra are similar to those seem in previous studies of thin gold films. Remodeling does not occur for films heated in a vacuum, immersed in solvent, or exposed to gases carrying saturated condensable vapor. Remodeling also occurs for other condensable vapors including water. Intermittent exposure of the films to ambient humidity followed by heating in house N_2 gas also leads to remodeling. These observations are rationalized by a theoretical model of capillary condensation and partial flooding of the films' nanoscale pore spaces, leading to attractive capillary forces that draw the gold nanoparticles into intimate contact and accelerate the coalescence process.

Introduction

Thin metal films manifest many different nanoscale morphologies, including hillocks (small metal hills that rise above the metal film), holey films (continuous films perforated by holes), and island films (elongated metal particles with irregular shapes, either isolated or interconnecting). As a consequence, the optical, electrical, and chemical properties of ultrathin metallic coatings are especially varied and interesting,[1,2] suggesting possible applications in many kinds of optical and electromagnetic devices. Ultrathin metal films (thicknesses <20 nm) made, for example, by vapor deposition usually have discontinuous island structures with large surface areas. Indeed, island films of Au, Ag, and Cu have been extensively studied as substrates for surface-enhanced infrared absorption (SEIRA)[3] and surface-enhanced Raman scattering (SERS).[2,4,5]

However, a common problem with metal island films for use in SERS is their variability.[6,7] The most commonly used SERS substrates, electrochemically roughened electrodes and vapor-deposited metal island films, suffer from poor reproducibility in terms of the size and periodicity of their nanoscale features, which leads to undesirable variability of SERS enhancement from one surface to the next.[8−12] Patterning assisted by probe microscopy can address these issues but cannot easily be scaled up.[13] The fabrication of reproducible metal island films with tailored nanoscale morphology for SERS is thus highly desirable and an active area of research.[14]

Gold island films have been studied extensively and fabricated by several routes. The classic route is metal evaporation and vapor deposition.[15−20] Deposition of preformed gold clusters[21,22] can be used to create some mor-

* To whom correspondence should be addressed. E-mail: Scrivens@sc.edu.
[†] Department of Chemistry & Biochemistry.
[‡] Department of Chemical Engineering.

(1) Velev, O. D.; Tessier, P. M.; Lenhoff, A. M.; Kaler, E. W. *Nature* **1999**, *401*, 548.
(2) Tessier, P. M.; Velev, O. D.; Kalambur, A. T.; Lenhoff, A. M.; Rabolt, J. F.; Kaler, E. W. *Adv. Mater.* **2001**, *13*, 396.
(3) Miyake, H.; Ye, S.; Osawa, M. *Electrochem. Commun.* **2002**, *4*, 973.
(4) Sockalingum, G. D.; Beljebbar, A.; Morjani, H.; Angiboust, J. F.; Manfait, M. *Biospectroscopy* **1998**, *4*, S71.
(5) Mulvaney, S. P.; He, L.; Natan, M. J.; Keating, C. D. *J. Raman Spectrosc.* **2003**, *34*, 163.
(6) Rowe, J. E.; Shank, C. V.; Zwemer, D. A.; Murray, C. A. *Phys. Rev. Lett.* **1980**, *44*, 1770.
(7) Wood, T. H.; Zwemer, D. A.; Shank, C. V.; Rowe, J. E. *Chem. Phys. Lett.* **1981**, *82*, 5.
(8) Kneipp, K.; Kneipp, H.; Itzkan, I.; Dasari, R. R.; Feld, M. S. *Chem. Rev.* **1999**, *99*, 2957.
(9) Busby, C. C.; Creighton, J. A. *J. Electroanal. Chem.* **1982**, *140*, 379.
(10) Taylor, C. E.; Pemberton, J. E.; Goodman, G. G.; Schoenfisch, M. H. *Appl. Spectrosc.* **1999**, *53*, 1212.
(11) Seki, H. *J. Vac. Sci. Technol.* **1981**, *18*, 633.
(12) Mrozek, I.; Pettenkofer, C.; Otto, A. *Surf. Sci.* **1990**, *238*, 192.
(13) Huang, S. M.; Hong, M. H.; Luk'yanchuk, B. S.; Lu, Y. F.; Song, W. D.; Chong, T. C. *J. Vac. Sci. Technol., B* **2002**, *20*, 1118.
(14) Litorja, M.; Haynes, C. L.; Haes, A. J.; Jensen, T. R.; Van Duyne, R. P. *J. Phys. Chem. B* **2001**, *105*, 6907.
(15) Zhang, L.; Cosandey, F.; Persaud, R.; Madey, T. E. *Surf. Sci.* **1999**, *439*, 73.
(16) Brune, H. *Surf. Sci. Rep.* **1998**, *31*, 121.
(17) Frechette, V. D.; Pulver, J. C.; Rossington, D. R. *J. Am. Ceram. Soc.* **1981**, *64*, 463.
(18) Pulver, J. C. Coalescence of Thin Films of Gold Condensed on Glass. Ph.D. Dissertation, Alfred University, Alfred, NY, 1973.
(19) Blum, B.; Salvarezza, R. C.; Arvia, A. J. *J. Vac. Sci. Technol., B* **1999**, *17*, 2431.
(20) Ye, G. X.; Xia, A. G.; Gao, G. L.; Lao, Y. F.; Tao, X. M. *Phys. Rev. B* **2001**, *63*, 125405.
(21) Bardotti, L.; Prével, B.; Treilleux, M.; Mélinon, P.; Perez, A. *Appl. Surf. Sci.* **2000**, *164*, 52.
(22) Koga, K.; Takeo, H. *Eur. Phys. J. D* **1999**, *9*, 535.

10.1021/cm051127w CCC: $30.25
Published on Web 09/10/2005

phologies not observed in vapor-deposited films. Electric fields have been used to make continuous gold films with holes[23] or hillocks.[24] Various templating and stenciling methods have also been investigated.[2,25−28]

Regardless of the synthesis route, solvent immersion and drying of metal island films is known to cause significant changes in their morphology and optical properties.[29−32] Thus, it is common to "stabilize" these films by sequential immersion and drying if they are to be used in applications (such as SERS) involving exposure to solvents. This ensures that observed changes in the films' optical properties are due to the "target" phenomenon (such as adsorption of a solute) rather than alteration of the metal island film itself. Stabilization by solvent immersion and drying usually follows thermal annealing, which is also commonly used to control island film morphology.

For the case of gold island films, Doron-Mor et al.[32] noted "spectral changes...attributed to the effect of wetting and drying on the fine morphology of the Au islands", so they routinely stabilized their Au films by immersion in 1:1 $CHCl_3$/EtOH followed by drying in N_2. This stabilization process did not produce any observable morphological changes but did result in a marked change in the films' UV−vis spectra.

Solvent-induced morphology changes have been studied more extensively in the case of silver island films.[30−32] Following on from earlier observations of adsorbate-induced morphological changes of Ag island films,[33,34] more recent studies clearly show that solvent evaporation controls island film "remodeling". For example, Roark and Rowlen[29] report that "close examination of the Ag islands..., after dipping in [acetone solution of] benzoic acid, indicates that a large number of Ag islands have been 'shoved' together, forming larger islands with distinct peaks". A subsequent, comprehensive study quantified solvent-induced morphology changes[30] using atomic force microscopy (AFM) and UV−vis spectrophotometry. In general, solvent evaporation resulted in increasing island height and aspect ratio (height/diameter), decreasing island area density (number/area), and decreasing optical absorption wavelength (λ_{max}). The value of λ_{max} decreased continuously with time as the solvent evaporated. The magnitude of the λ_{max} decrease was greater for MeOH than acetone, and much greater when the solvent was water. Comparing the λ_{max} blue shift for dried films with values for immersed films, the authors noted that "the withdrawal process plays a significant role in the modification of Ag film morphology" and that "the blue shift in the optical spectrum of a [silver island film] dipped into a volatile solvent is attributed to perturbation in surface morphology".

Although this phenomenon has been noted for some time, the underlying mechanism of solvent-induced remodeling of metal island films has not been explored. Malinsky et al., in their study of silver island films made by Ag nanoparticle deposition,[31] concluded that "the dominant factor in water (solvent) induced nanoparticle reconstruction is likely to be the strong decrease in surface tension at the hydrophilic glass-water interface". In essence, they hypothesize that changing the ambient environment from air to water alters the balance of interfacial tensions to favor dewetting of glass by Ag. While certainly valid, this argument does not address the kinetics of the remodeling process.

We discovered, fortuitously, that vapor-deposited gold island films are remodeled upon exposure to solvent vapor. A heated glass slide coated with a thin gold film was partially immersed in styrene in an attempt to polymerize a thin layer of polystyrene on top of the gold. We noticed that the portion of the gold-coated film that had not been immersed in the styrene turned pink. Examination by environmental scanning electron microscopy (ESEM) revealed no apparent change in the morphology of the immersed portion of the film, but significant remodeling of the portion that had been exposed to vapor.

This discovery led to the more thorough investigation reported here. We report results from a systematic study of vapor-assisted remodeling of gold films with morphology characterized by ESEM and AFM, and optical properties by UV−vis spectrophotometry. Different film morphologies (islands, interconnected networks, holey continuous films) develop depending on the initial film thickness, film temperature, vapor composition, and time. The features of the UV−vis spectra vary with the film morphology in ways that are in accord with previous studies of gold island films. The high interfacial tension of the gold−glass interface clearly favors the dewetting of the glass by gold. To rationalize the kinetics of the remodeling process, we utilize an existing theoretical model[35] to describe capillary condensation of vapor between neighboring gold nanoparticles in the film. For condensable vapors below saturation, partial flooding and the resulting menisci create strong, attractive capillary forces that we believe control the kinetics of the remodeling process and promote coalescence of the films' constituent gold nanoparticles.

Experimental Section

Gold Film Preparation. Gold films were deposited on glass microscope slides (30 × 10 × 1.2 mm, Fisher) by thermal evaporation of gold wire (99.9+% pure, Aldrich) held in a tungsten boat, at a pressure of about 1×10^{-5} Torr. The deposition rate was about 0.34 Å/s. The average gold film thickness was determined using a quartz crystal microbalance (SQM-160 rate/thickness monitor, Sigma Instruments, Inc.) installed next to the slide holder.

(23) Perea-Lopez, N.; Rakov, N.; Xiao, M. F. *Rev. Sci. Instrum.* **2002**, *73*, 4399.
(24) Xiao, M. F. *Mater. Lett.* **2002**, *52*, 301.
(25) Meli, M.-V.; Lennox, R. B. *Langmuir* **2003**, *19*, 9097.
(26) Zehner, R. W.; Sita, L. R. *Langmuir* **1999**, *15*, 6139.
(27) Zehner, R. W.; Lopes, W. A.; Morkved, T. L.; Jaeger, H.; Sita, L. R. *Langmuir* **1998**, *14*, 241.
(28) Thurn-Albrecht, T.; Steiner, R.; DeRouchey, J.; Stafford, C. M.; Huang, E.; Bal, M.; Tuominen, M.; Hawker, C. J.; Russell, T. P. *Adv. Mater.* **2000**, *12*, 787.
(29) Roark, S. E.; Rowlen, K. L. *Anal. Chem.* **1994**, *66*, 261.
(30) Roark, S. E.; Semin, D. J.; Lo, A.; Skodjc, R. T.; Rowlen, K. L. *Anal. Chim. Acta* **1995**, *307*, 341.
(31) Malinsky, M. D.; Kelly, K. L.; Schatz, G. C.; Van Duyne, R. P. *J. Am. Chem. Soc.* **2001**, *123*, 1471.
(32) Doron-Mor, I.; Barkay, Z.; Filip-Granit, N.; Vaskevich, A.; Rubinstein, I. *Chem. Mater.* **2004**, *16*, 3476.
(33) Von Raben, K. U.; Dorain, P. B.; Chen, T. T.; Chang, R. K. *Chem. Phys. Lett.* **1983**, *95*, 269.
(34) Murray, C. A.; Bodoff, S. *Phys. Rev. B* **1985**, *32*, 671.
(35) Lin, F.; Meier, D. J. *Langmuir* **1995**, *11* (7), 2726.

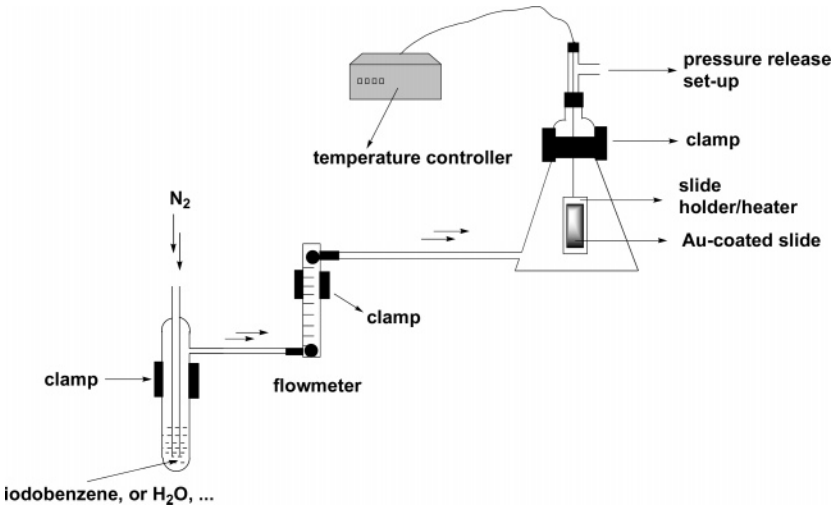

Figure 1. Experimental apparatus for vapor-induced remodeling of metal films.

All initial film thicknesses reported in this paper are average or nominal values. The glass slides were precleaned by immersion in fresh piranha solution (30% H_2O_2, 70% H_2SO_4 by volume) for 3−4 h, followed by rinses with copious amounts of deionized water and ethanol. The clean slides were dried under nitrogen and kept in a desiccator prior to use.

We obtain nitrogen gas from a departmental liquid nitrogen storage tank. The boil-off from this tank is distributed to all of the laboratories in the building. The supplier of this system states that the upper limit of water contamination in this system is 3 ppm. Although we assume the house N_2 gas to be nominally dry, we cannot rule out the possibility that it contains trace amounts of water vapor.

Vapor Exposure Apparatus. Gold island films were exposed to vapor in the apparatus shown in Figure 1. The gold-coated glass slide is mounted on a slide holder in an enclosed flask. The slide holder also serves as a heater with external, calibrated temperature control. Nitrogen gas passes through a bubbler tube at room temperature holding the solvent of interest. The solvent evaporates and is carried by the nitrogen through the flow meter and into the flask holding the heated gold film. The nitrogen−vapor mixture passes out of the flask through a back-pressure valve.

Environmental Scanning Electron Microscopy. All ESEM images of gold films were taken with a Quanta 200 ESEM instrument (FEI, Inc.) at room temperature and in low-vacuum mode with a chamber pressure of 0.90 Torr. Accelerating voltages of 20 or 30 kV were usually applied with a working distance of 5−10 mm. Under these conditions, the image resolution is about 3.5 nm. Image analysis was carried out using NIH image processing software, ImageJ 1.32j (Wayne Rasbanc, National Institutes of Health, http://rsb.info.nih.gov/ij).

Atomic Force Microscopy. All AFM images were acquired at ambient temperature and atmosphere using the acoustically driven tapping mode, abbreviated below as TMAFM (PicoSPM, Molecular Imaging, Inc.). We used standard silicon AFM probes (Mikromasch Ultrasharp NSC35/AlBS) having cantilever spring constants of 2.5−12.5 N/m and resonance frequencies from 120 to 240 kHz. The manufacturer estimates that the probe tip radius of curvature is no smaller than about 5−10 nm. Our measurements employed a "small" 6 μm piezoelectric z-scanner (Molecular Imaging) calibrated by the manufacturer using calibration gratings with step heights of 20, 100, and 500 nm to precisely quantify any vertical nonlinearity of the scanner. According to the manufacturer, this scanner has a minimum vertical resolution of 0.01 nm. Topology images were analyzed using commercial image analysis software (SPIP with Grain Module, Image Metrology) to identify distinct surface features assumed to be individual gold island particles.

UV−Vis Spectrophotometry. UV−vis absorption spectra were acquired on a Varian Cary 500 UV−vis−near-IR spectrophotometer at room temperature in N_2 in the wavelength range of 400−1100 nm. The scan rate was 600 nm/min. The bandwidth of the light source in the UV−vis region was 2 nm. A baseline correction was executed prior to each measurement session consisting of measurements on five randomly selected regions of a given film. The gold-coated glass slide was mounted in a slide holder perpendicular to the incident light beam with the gold-coated side facing the incident beam. Five independent spectra were acquired for each sample to ensure reproducibility, although only one spectrum for each sample is shown here.

Results and Discussion

Time Dependence. A gold-coated glass slide (10 nm nominal thickness) was exposed to N_2 carrying iodobenzene vapor. The slide temperature was maintained at 120 °C during the exposure. At different times, the slide was cooled, removed from the flask and holder, and characterized by ESEM and UV−vis spectrophotometry. Before reheating and continuing the vapor exposure, the glass slide was remounted and the flask was purged with house N_2 gas.

Morphology. Figure 2 shows ESEM images of the 10 nm gold film before exposure and after 5 min, 30 min, and 5 h of exposure to iodobenzene vapor. The ESEM image of the gold film before vapor exposure (Figure 2a) does not show any large-scale morphological features at 40000× magnification (2 μm scale bar in Figure 2a). However, close examination of an enlarged portion of the image (Figure S1, Supporting Information) shows a fine granular structure suggesting close-packed, nanometer-scale particles. After 5 min of exposure to iodobenzene vapor, the ESEM image (Figure 2b) shows that the film morphology has been remodeled into one dominated by interconnected gold domains. After 30 min of exposure (Figure 2c), the gold domains have become discontinuous islands. Beyond this point, the rate of change of the island morphology slows. After 5 h of exposure (Figure 2d), the gold islands have further consolidated, revealing more of the underlying glass slide. The morphology of another film exposed to vapor for

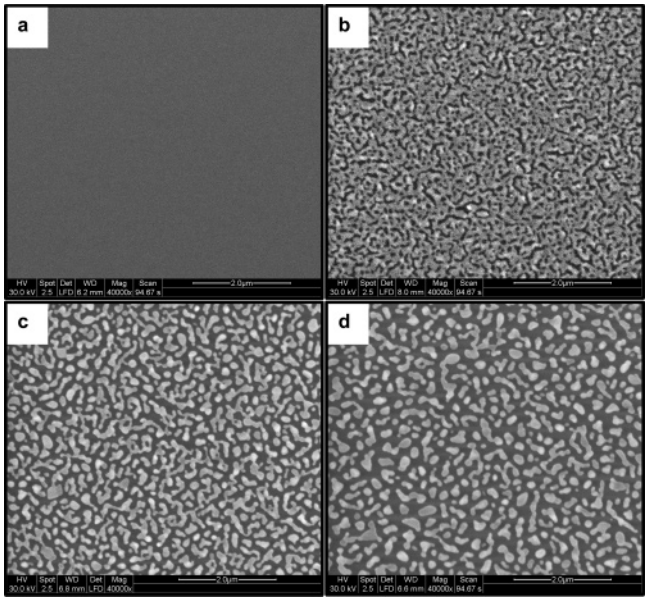

Figure 2. ESEM images of a gold film on glass (10 nm initial thickness) exposed to iodobenzene vapor for (a) 0 min, (b) 5 min, (c) 30 min, and (d) 300 min. The slide was maintained at 120 °C during the exposure, and the N_2 carrier gas flow rate was 0.20 L/min. The scale bar in each image is 2.0 μm.

24 h exposure (Figure S2, Supporting Information) does not appear to differ much from the image of the film exposed for 5 h.

Image analysis quantifies the extent of gold dewetting of the glass slide. Assuming that the gold coverage of the glass prior to exposure is 100%, the area covered by gold decreases to 71.4%, 48.8%, and then 37.1% after exposure times of 5 min, 30 min, and 5 h, respectively. The distribution of gold island areas also shifts to smaller values as the exposure time increases from 5 to 30 min (Figure S3, Supporting Information). More detailed statistics extracted from the images in Figure 2 are tabulated in the Supporting Information (Table S1).

As the gold dewets the glass and forms islands, the vertical dimension of the gold domains must increase (assuming no significant loss of gold due to evaporation). TMAFM measurements confirm this (Figure 3). Before vapor exposure, the TMAFM topography image (Figure 3a) shows that the 10 nm gold film consists of small, closely packed gold nanoparticles that are just visible in the corresponding ESEM image (Figure 2a, enlarged version given in Figure S1). Because of tip convolution and the packing of the nanoparticles, it is difficult to find a baseline that definitively corresponds to the glass surface. Nevertheless, a typical vertical cross-section for this film (Figure 3c) shows that the characteristic vertical distance between the highest and lowest points on the cross-section is on the order of 10 nm, in agreement with the nominal 10 nm film thickness based

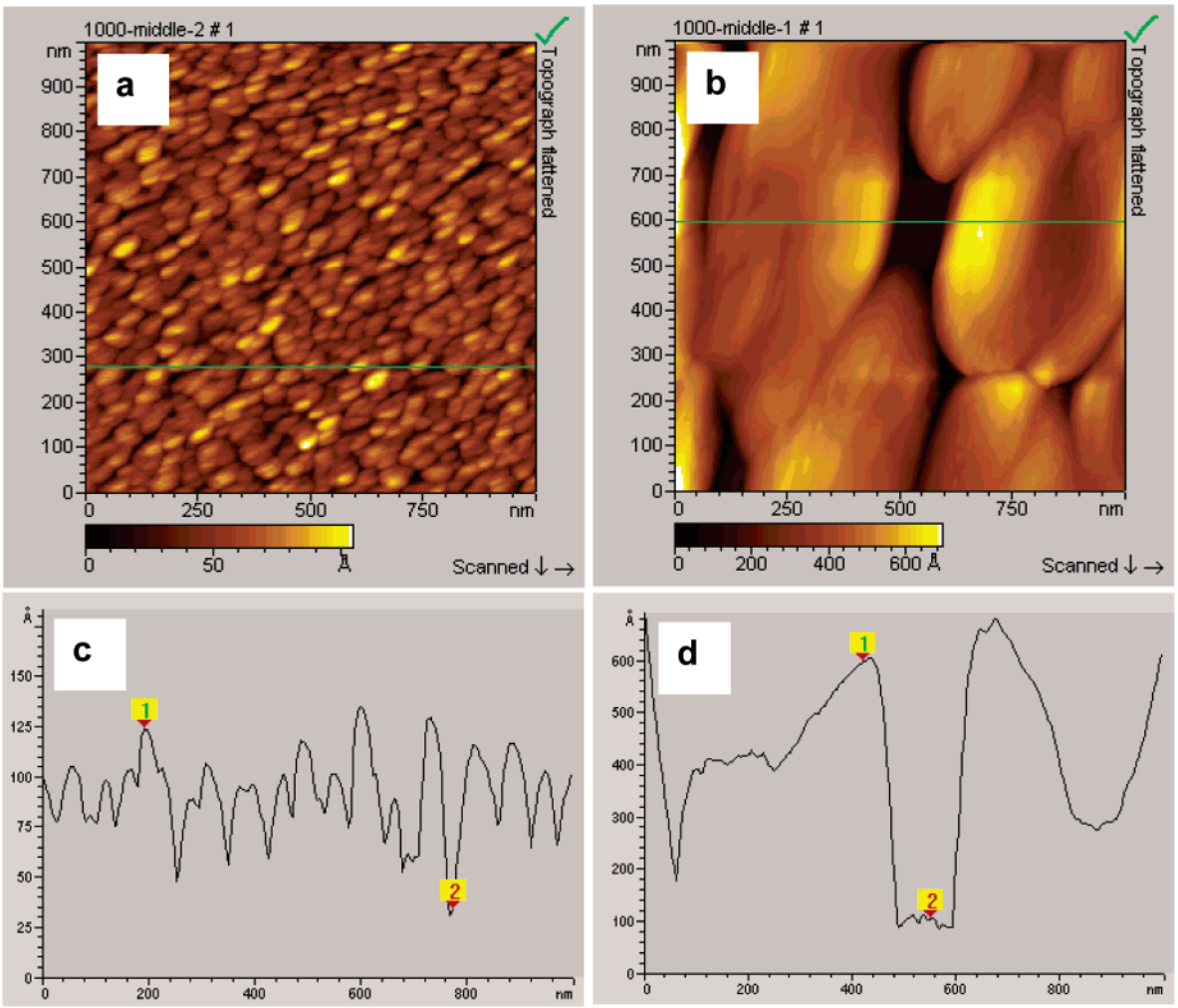

Figure 3. TMAFM topography images of a gold film (10 nm nominal thickness) on glass (a) before exposure and (b) after 24 h of exposure to iodobenzene vapor. Other exposure conditions are as in Figure 2. Panels c and d show vertical cross-sections along the horizontal lines in panels a and b, respectively.

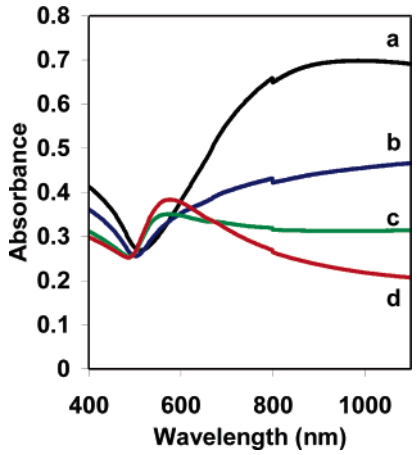

Figure 4. UV−vis spectra of the 10 nm gold film on glass, exposed to iodobenzene vapor for (a) 0 min, (b) 5 min, (c) 30 min, and (d) 300 min. Other exposure conditions are as in Figure 2.

on QCM measurement. After 24 h of exposure to iodobenzene vapor, the TMAFM topography image (Figure 3b) shows large elevated domains that have (qualitatively) the same shape as the gold islands seen in the corresponding ESEM image (Figure S2b, Supporting Information, similar to Figure 2d). The selected vertical cross-section (Figure 3d) shows that the vertical distance between the highest and lowest points has increased to as much as 60 nm. The average vertical height of the gold island features in Figure 3b is 26 nm.

The ESEM and TMAFM observations are consistent with the view that exposure of the gold films to iodobenzene vapor leads to coalescence of gold nanoparticles into larger gold islands. We refer to this phenomenon as remodeling of the gold film. This remodeling does not occur when the film is heated under vacuum conditions (vide infra). Remodeling does occur when the films are exposed to condensable vapors including water (vide infra), DMF, styrene, and several others.

The chemical integrity of gold films exposed to iodobenzene vapor was confirmed by X-ray photoelectron spectroscopy (XPS). XPS spectra were collected from an unexposed 5 nm gold film and one maintained at 120 °C and exposed to iodobenzene vapor for 24 h (TMAFM images of these films will be shown later). Survey scans (Figure S4, Supporting Information) show no evidence of carbon, iodine, or other elements in the film. This result suggests that no chemical reactions occurred yielding products that remained on the film.

UV−Vis Spectra. The UV−vis spectrum of the initial, unexposed 10 nm gold film (Figure 4) displays a broad absorption band centered at 985 nm and a minimum absorbance at 512 nm, but no surface plasmon absorption peak in the visible region. These spectral features are consistent with those of a continuous thin film.[36] However, the TMAFM image of this gold film (Figure 3a) clearly shows closely packed gold nanoparticles. Thus, the surface plasmon modes of these particles must be coupled, perhaps contributing to the broad absorbance peak centered at 985 nm. After exposure to iodobenzene vapor for 5 min, the film's UV−vis spectrum manifests a minimum at 501 nm and decreased absorbance in the near-IR region, but no evidence of a surface plasmon resonance. These spectral features are consistent with the observed film morphology consisting of interconnected domains that have not quite separated into discrete islands.[36−39]

The signature of a surface plasmon resonance (a maximum at 575 nm) appears in the spectrum of the 10 nm gold film exposed to vapor for 30 min. This peak is responsible for the film's pink-violet color.[40,41] The emergence of the surface plasmon resonance peak is consistent with the observation (Figure 2c) that the gold film now manifests discrete islands.[42] The spectrum for the film exposed for 5 h (Figure 4d) shows growth of the surface plasmon resonance but little shift of its peak (575 nm). We expect to see these kinds of changes as the gold islands' size and shape distributions become narrower. The next section gives further discussion of the relationship between UV−vis spectral features and gold island size and shape distributions in the context of varying initial film thickness.

Temperature Dependence. Time-dependent remodeling of gold film morphology also occurs when the film is held at lower temperatures. We have carried out extensive measurements of film morphology (by ESEM) and UV−vis spectrophotometry for gold films maintained at temperatures between 60 and 120 °C. Detailed results are presented elsewhere.[43] In general, lower temperatures generally slow the rate of film remodeling. Further experiments are needed to see if low-temperature, long-time exposure leads to the same final morphology and UV−vis spectra as high-temperature, short-time exposure. We observe no vapor-assisted remodeling for unheated films at the same ambient temperature as the vapor-laden N_2 carrier gas.

The next section focuses on the effect of varying initial film thickness on morphology. The time dependence of the UV−vis absorbance depends strongly on the initial, nominal gold thickness and is discussed at the end of the next section.

Varying Initial Film Thickness. *Morphology.* Gold films with varying nominal thicknesses (5, 10, 15, and 20 nm) were deposited on glass slides, heated to 120 °C, and exposed for 30 min to iodobenzene vapor carried by N_2. ESEM images of these films before vapor exposure (5 and 10 nm films, Figure S1, Supporting Information, others not shown) show only a fine, granular structure that is just visible at 40000× magnification. Figure 5 displays ESEM images of these four gold films after 30 min of vapor exposure. The morphology of the 5 nm gold film has been remodeled (Figure 5a) and now shows a high density of small circular or elliptical islands with an average Feret diameter[44] of 109

(36) Kreibig, U.; Genzel, L. *Surf. Sci.* **1985**, *156*, 678.
(37) Kalyuzhny, G.; Vaskevich, A.; Schneeweiss, M. A.; Rubinstein, I. *Chem.—Eur. J.* **2002**, *8*, 3850.
(38) Papavassiliou, G. C. *Prog. Solid State Chem.* **1979**, *12*, 185.
(39) Norrman, S.; Andersson, T.; Granqvist, C. G. *Phys. Rev. B* **1978**, *18*, 674.
(40) Swami, A.; Kasture, M.; Pasricha, R.; Sastry, M. *J. Mater. Chem.* **2004**, *14*, 709.
(41) Frederix, F.; Friedt, J.-M.; Choi, K.-H.; Laureyn, W.; Campitelli, A.; Mondelaers, D.; Maes, G.; Borghs, G. *Anal. Chem.* **2003**, *75*, 6894.
(42) Link, S.; El-Sayed, M. A. *J. Phys. Chem. B* **1999**, *103*, 8410.
(43) Luo, Y. A New Method of Making Gold Island Films. Ph.D. Dissertation, University of South Carolina, Columbia, SC, 2004.
(44) The Feret diameter is the maximum separation of two points on the boundary of a discrete object.

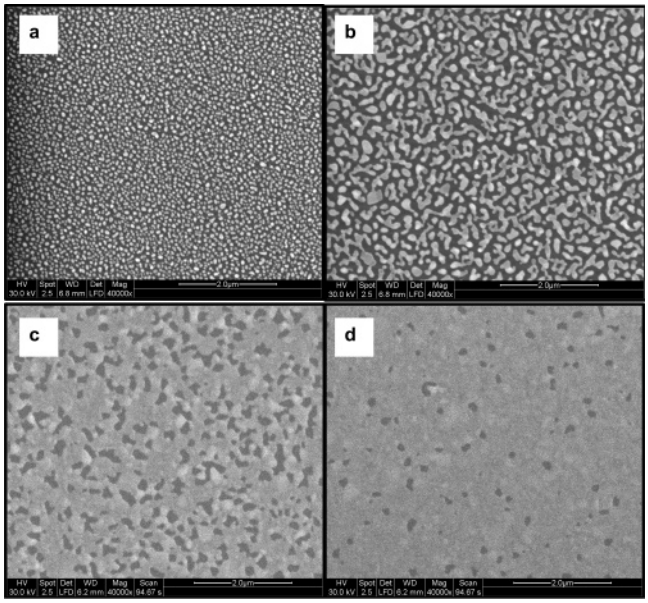

Figure 5. ESEM images of gold films of varying initial thicknesses on glass exposed to iodobenzene vapor for 30 min. The nominal initial thicknesses were (a) 5 nm, (b) 10 nm, (c) 15 nm, and (d) 20 nm. The slides were maintained at 120 °C during the exposure, and the N_2 carrier gas flow rate was 0.20 L/min. The scale bar in each image is 2.0 μm.

nm. Longer vapor exposure did not lead to further changes in the morphology of the 5 nm gold film (Figure S5, Supporting Information). The TMAFM topography images of the 5 nm gold film (Figure 6) show that the initial film (Figure 6a) consists of densely packed gold nanoparticles (average particle height approximately 5 nm, Figure 6c). Upon exposure to iodobenzene vapor, the gold nanoparticles apparently coalesce into a smaller number of taller gold islands (Figure 6b,d). This observation is consistent with the trends seen for the 10 nm gold films (Figure 3).

The morphology of the 10 nm gold film after 30 min of vapor exposure (Figure 5b) differs considerably from that of the 5 nm film. The islands appear to be more elongated and irregularly shaped, and many of them are interconnected. The average Feret diameter of the islands in Figure 5b is 401 nm. For the gold films with initial thicknesses of 15 and 20 nm, 30 min of vapor exposure does not lead to island formation, but continuous films with many holes (Figures 5c,d). The number of holes and their average area decrease with increasing initial film thickness. Complete statistics describing the morphology of these films are easily extracted by image analysis and are tabulated in the Supporting Information (Table S2, Figure S6).

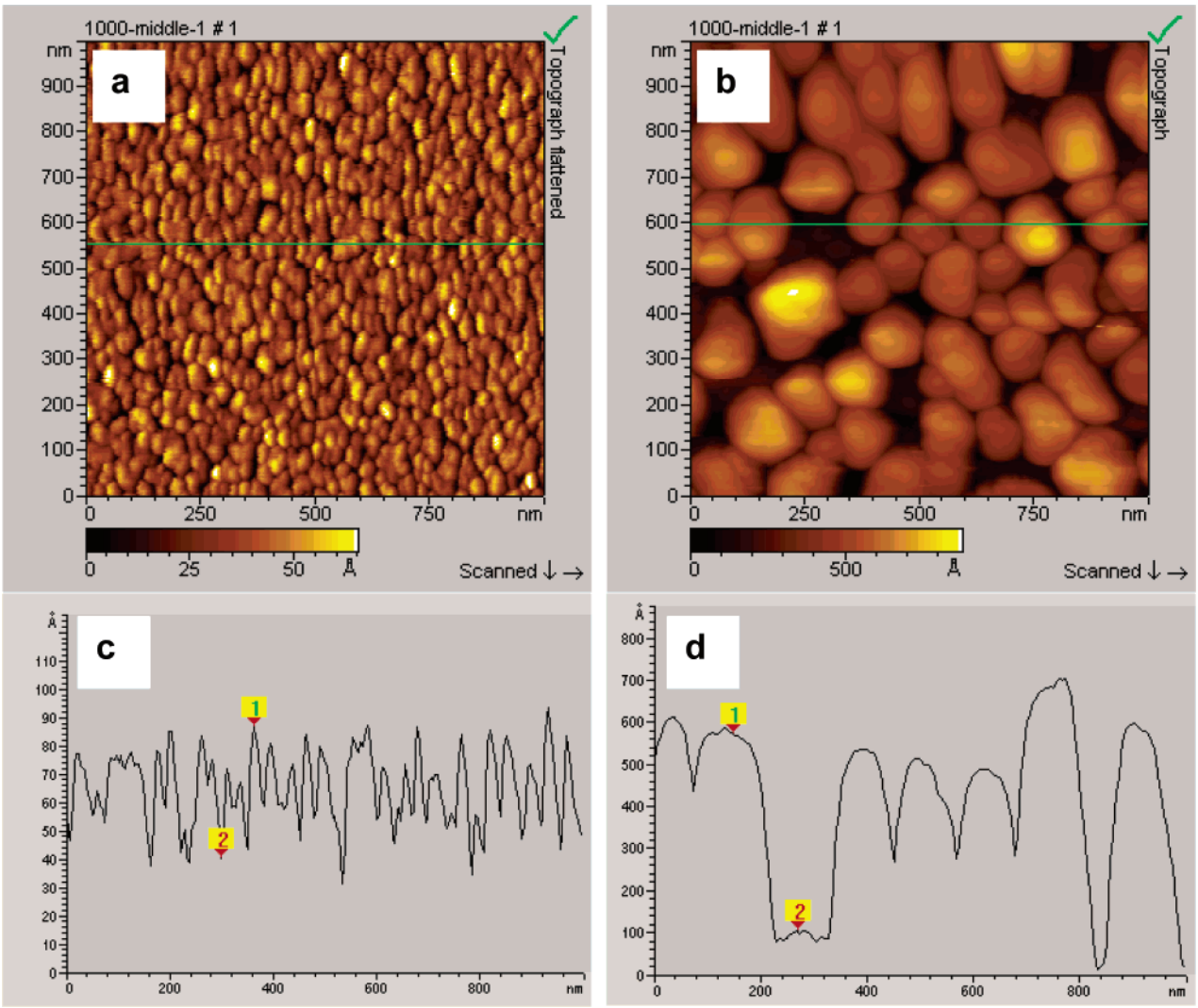

Figure 6. TMAFM topography images of a gold film (5 nm nominal thickness) on glass (a) before exposure and (b) after 24 h of exposure to iodobenzene vapor. Other exposure conditions are as in Figure 2. Panels c and d show vertical cross-sections along the horizontal lines in panels a and b, respectively.

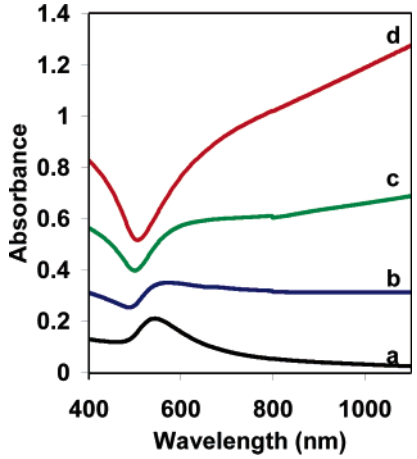

Figure 7. UV−vis spectra of gold films of varying initial thicknesses on glass exposed to iodobenzene vapor for 30 min. The nominal initial thicknesses were (a) 5 nm, (b) 10 nm, (c) 15 nm, and (d) 20 nm. Other exposure conditions are as in Figure 5.

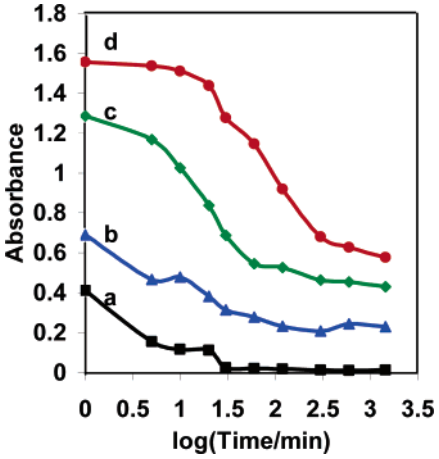

Figure 8. Time dependence of absorbance at 1100 nm for gold films with different initial thicknesses. The nominal initial thicknesses were (a) 5 nm, (b) 10 nm, (c) 15 nm, and (d) 20 nm. Other exposure conditions are as in Figure 5.

UV−Vis Spectra. Absorption spectra for the initial, unexposed films with varying nominal thicknesses are shown in the Supporting Information (Figure S7). All of the UV−vis spectra show a minimum absorbance at wavelengths between 509 and 512 nm. The spectrum for the 5 nm film has a broad adsorption maximum centered at 798 nm, like that seen for the 10 nm film (Figure 4). This maximum may arise from the coupling of the surface plasmon modes of the constituent gold nanoparticles. However, none of the initial, unexposed films showed any evidence of a distinct surface plasmon resonance attributable to individual gold nanoparticles. The thicker films simply show absorbance increasing continually through the near-IR part of the spectrum. Absorbance increases with nominal film thickness at all wavelengths, as would be expected.

Figure 7 shows the UV−vis spectra for the four exposed films displayed in Figure 5. The spectrum for the 5 nm gold film shows a well-developed surface plasmon resonance peak centered at 544 nm. The presence of this peak is consistent with the appearance of discrete, relatively uniform gold islands in the ESEM image (Figure 5a). The spectrum for the 10 nm film (Figure 4c or 7b) has a surface plasmon resonance centered at 575 nm, but the peak is less symmetric and quite broad, extending well into the near-IR region. The Supporting Information shows plots (Figure S8) giving a magnified view of the surface plasmon peaks for the 5 and 10 nm films. The red shift, broadening, and asymmetry of the surface plasmon peak for the 10 nm film (relative to the 5 nm film) are likely due to the 10 nm film's increased island size[37,38,42] as well as the broader distribution of island size and shape.[40,45−47]

An even closer look at the 530−730 nm region of the spectrum for the 10 nm film (Figure S9) reveals a small shoulder peak centered at 675 nm, probably arising from highly elongated islands just on the verge of connectivity. The spectral features of these elongated islands resemble those of aggregated gold particles.[36,38,42,48] If this hypothesis is correct, then the shoulder peak at 675 nm corresponds to the longitudinal plasmon resonance, while the main peak centered at 575 nm corresponds to the transverse plasmon resonance.[32,49]

The UV−vis spectra for the 15 and 20 nm gold films (Figure 7c,d) do not show a well-defined surface plasmon resonance peak in the visible region. The minima in the spectra for the 15 and 20 nm films (at 500 and 506 nm, respectively) are consistent with previous observations of minima between 510 and 550 nm for continuous gold films with a small amount of roughness.[37,39] The approximately linear increase in absorbance with increasing film thickness at wavelengths greater than 540 nm has been observed in many previous studies.[32,37,40,50−54] The broad absorption at wavelengths greater than 600 nm and into the near-IR spectral region is characteristic of continuous films.[36,37,39]

Figure 8 shows the time dependence of the absorption at a fixed wavelength, 1100 nm, for gold films of different initial thicknesses. For all of the films, the absorbance changes most rapidly in the first 30 min. The absorbance of the 15 and 20 nm films continues to change even after several hours of vapor exposure, implying that the dynamics of the remodeling process slow considerably for films with initial thicknesses exceeding some critical value. The time dependence of the remodeling dynamics can also be seen in the initial slope of the absorbance versus time, dA/dt. Normalizing the initial slope with that of the 5 nm film, the relative values of dA/dt are 0.89, 0.46, and 0.08 for the 10, 15, and 20 nm films. This indicates that the remodeling process starts more slowly as the initial film thickness increases.

(45) Mulvaney, P. *Langmuir* **1996**, *12*, 788.
(46) Bohren, C. F.; Huffman, D. R. *Absorption and Scattering of Light by Small Particles*; Wiley: New York, 1983.
(47) Mayya, K. M.; Gole, A.; Jain, N.; Phadtare, S.; Langevin, D.; Sastry, M. *Langmuir* **2003**, *19*, 9147.
(48) Liao, J. H.; Zhang, Y.; Yu, W.; Xu, L,; Ge, C. W.; Liu, J. H.; Gu, N. *Colloids Surf., A* **2003**, *223*, 177.
(49) Kumar, A.; Mandale, A. B.; Sastry, M. *Langmuir* **2000**, *16*, 6921.
(50) Kalyuzhny, G.; Vaskevich, A.; Ashkenasy, G.; Shanzer, A.; Rubinstein, I. *J. Phys. Chem. B* **2000**, *104*, 8238.
(51) Swami, A.; Kumar, A.; Selvakannan, P. R.; Mandal, S.; Sastry, M. *J. Colloid Interface Sci.* **2003**, *260*, 367.
(52) Swami, A.; Kumar, A.; D'Costa, M.; Pasricha, R.; Sastry, M. *J. Mater. Chem.* **2004**, *14*, 2696.
(53) Švorčík, V.; Zehentner, J.; Rybka, V.; Slepièka, P.; Hnatowicz, V. *Appl. Phys. A* **2002**, *75*, 541.
(54) Krasteva, N.; Besnard, I.; Guse, B.; Bauer, R. E.; Mullen, K.; Yasuda, A.; Vossmeyer, T. *Nano Lett.* **2002**, *2* (5), 551.

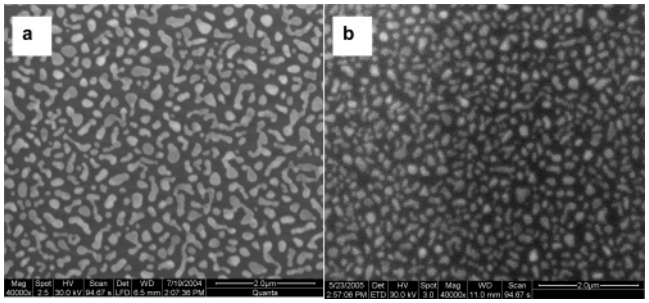

Figure 9. ESEM images of gold films on glass (10 nm initial thickness) exposed to (a) iodobenzene vapor for 24 h and (b) water vapor for 18 h. The slide was maintained at 120 °C during the exposure, and the N_2 carrier gas flow rate was 0.20 L/min. The scale bar in each image is 2.0 μm.

In summary, the thicker gold films have all of the optical characteristics of rough but continuous films, consistent with the morphology seen in the ESEM images. As the initial thickness decreases, absorbance decreases at all wavelengths, and the surface plasmon peak appears and becomes more distinct. These trends reflect the transition of the film morphology from continuous to partially continuous to discontinuous island morphology, as seen in the ESEM images.

Varying Vapor Composition. Condensable vapors below saturation are a prerequisite for remodeling. We observe no evidence of remodeling for gold films heated and immersed in liquids, nor for gold films exposed to gases carrying condensable vapors at saturation conditions (i.e., 100% relative humidity).

So far in this paper, all of the reported results are from experiments that employed iodobenzene vapor to remodel gold films. Iodobenzene seems to be nonreactive and gives a relatively fast rate of film remodeling, so we have used it as the preferred "remodeling agent" in our work to date. However, condensable vapors of some other solvents also have been used to remodel gold films. For example, Figure 9 compares ESEM images of 10 nm gold films remodeled with iodobenzene vapor and with water vapor. Although the exposure times differed, the morphologies of the two films after exposure are qualitatively similar.

Glass slides coated with 5 nm gold films were heated to 60 °C and exposed to vacuum, house N_2 gas, water vapor, and iodobenzene vapor (the latter two carried by N_2 gas at laboratory ambient temperature). Periodically, the films were cooled, removed from the flask, and characterized by UV−vis spectrophotometry. Figure 10 shows the absorbance at 1100 nm for the various films as a function of exposure time. The film exposed to vacuum shows a small change in absorbance initially, and then almost no further change over a 10 h period. This result shows that thermal annealing is not responsible for the remodeling observed in films exposed to vapors at elevated temperatures. The film exposed to iodobenzene vapor undergoes rapid remodeling with most of the absorbance decrease complete within the first 30 min of exposure. The film exposed to water vapor shows a relatively slow decrease in absorbance at 1100 nm. This result indicates that water vapor is effective at remodeling gold films, but that the remodeling process would take much longer than 10 h to complete for 5 nm films maintained at 60 °C.

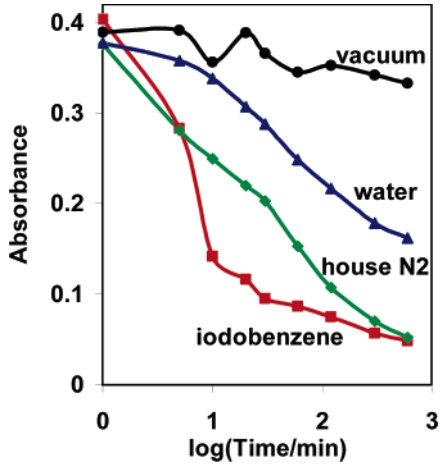

Figure 10. Time dependence of absorbance at 1100 nm for gold films exposed to vacuum, house N_2 gas, water vapor carried by N_2, and iodobenzene vapor carried by N_2. The initial gold film thicknesses were 5 nm, and the film temperature was maintained at 60 °C.

Finally, Figure 10 indicates that the gold film exposed to house N_2 gas shows a significant decrease in absorbance at 1100 nm over the course of 10 h. This implies that house N_2 gas leads to significant remodeling of gold film morphology. This may be counter to intuition since condensation of liquid N_2 on these films is impossible: the film temperature is greater than nitrogen's critical temperature. However, one must remember that these films were exposed to ambient humidity before they were mounted in the flask, as well as each time they were cooled and removed from the flask for measurement of the UV−vis spectrum. Moreover, the house N_2 gas may also contain as much as 3 ppm water. This would certainly lead to significant capillary condensation of water on the films every time the films came in contact with the laboratory atmosphere. Exposure to vacuum might lead to rapid removal of capillary water before significant remodeling could occur. Exposure of the film to N_2 gas would also remove capillary water, but at a much slower rate. Comparing the absorbance versus time curves for films exposed to iodobenzene vapor and house N_2 gas (Figure 10), 10 h exposure leads to the same absorbance value, suggesting that these films have the same final morphology. However, the rate of absorbance decrease with time is significantly slower for the film exposed to house N_2 gas. The theoretical analysis presented in the next section provides further support for this explanation as well as a proposed general mechanism for vapor-assisted remodeling of metal island films.

Theoretical Analysis. We think that both surface energetics and capillary forces play roles in the remodeling of the gold films observed in this study. We already know that the thermodynamics of the gold and glass surfaces favor dewetting of glass by gold. From textbook definitions[55] of cohesion and adhesion, the spreading coefficient (S) of gold (Au) on glass (G) in a vacuum is

$$S = \gamma_G^\circ - \gamma_{Au}^\circ - \gamma_{Au,G} \quad (1)$$

where γ_G° and γ_{Au}° are surface energies and $\gamma_{Au,G}$ represents the gold−glass interfacial energy. The surface energy of

(55) Hunter, R. J. *Foundations of Colloid Science*; Oxford University: Oxford, U.K., 1985; Vol. 1.

gold[56] (1.40 J/m^2) is higher than that of glass[57] (0.325 J/m^2 for soda lime glass, a typical value), so S has a negative value regardless of the value of $\gamma_{Au,G}$. This indicates a strong thermodynamic driving force for dewetting of the glass by the gold. Strong gold cohesion and weak gold−glass adhesion favor the coalescence of the gold nanoparticles into domains that minimize the gold surface area. However, the rate of gold film remodeling is very slow under vacuum conditions (Figure 10). The presence of vapor must somehow introduce another mechanism that governs the kinetics of the remodeling process.

The AFM images (Figures 3 and 6) clearly show that the initial 5 and 10 nm gold films consist of small grains with considerable nanoscale porosity. The same is presumably true for the thicker films as well. Capillary condensation of liquid in these pores will certainly occur in the presence of condensable vapors. Assuming that a liquid (L) film condenses around the glass−gold contact lines, the spreading coefficient in this case becomes

$$\begin{aligned} S &= \gamma_{G,L} + \gamma_{Au,L} - (\gamma_{Au,G} + 2\gamma_{Au}^{\circ}) \\ &= \gamma_{G}^{\circ} - \gamma_{Au}^{\circ} - \gamma_{Au,G} - \gamma_{L,vap}[\cos(\theta_{L,G}) + \cos(\theta_{L,Au})] \end{aligned} \quad (2)$$

where the second form employs the Young equation[55] to express the liquid−solid interfacial energies in terms of the liquid−glass and liquid−gold contact angles, $\theta_{L,G}$ and $\theta_{L,Au}$. For water and iodobenzene, both contact angles are between 0° and 90°, so the new terms in eq 2 make S even more negative. However, the liquid−vapor interfacial energies, $\gamma_{L,vap}$, are relatively small (0.0728 and 0.0397 J/m^2 for water and iodobenzene at 298 K, respectively[58]). Hence, the effect of capillary condensation on the spreading coefficient is not large enough to account for the observation of gold film remodeling in the presence of condensable vapor but not in a vacuum.

Nevertheless, we believe that capillary condensation plays a crucial role by creating attractive capillary forces that draw the gold nanoparticles into intimate contact and accelerate the sintering process. We hypothesize that the observed rate of remodeling should be proportional to the capillary force between neighboring gold nanoparticles. Lin and Meier[35] published a model for latex film formation driven by capillary forces between neighboring spherical particles. We have adapted their model to estimate the capillary force between gold nanoparticles within our films as a function of the relative humidity (RH) of the condensable vapor. The model estimates the attractive capillary force between two neighboring nanoparticles as a function of relative humidity. Various parameters, including the liquid−gold contact angle, liquid−vapor interfacial energy, and liquid molar density, are tabulated or readily measured. The model also requires a characteristic dimension of the nanoparticles, here assumed to be equal to the initial film thickness.

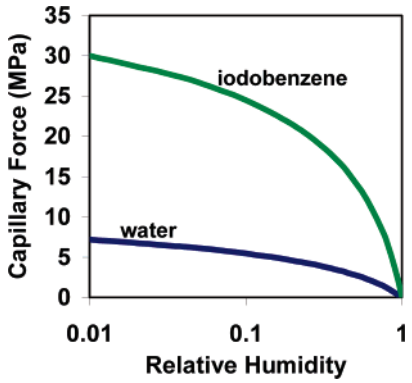

Figure 11. Theoretical estimate of the attractive capillary force between gold nanoparticles (5 nm characteristic size) as a function of the relative humidity (0 < RH < 1%) of the condensable vapor. The calculations utilize tabulated values[58] for the liquid molar volumes and liquid−vapor interfacial tensions for iodobenzene and water, and our own measured values for the contact angles of iodobenzene and water on the 5 nm gold film (0° and 81°, respectively).

Predictions of the model for 5 nm gold films exposed to iodobenzene and water vapors are given in Figure 11. At saturation (100% RH), the capillary pressures and forces are zero because the pores are flooded; according to the Kelvin equation,[55] the liquid meniscus assumes a configuration having zero net curvature. This prediction is consistent with our observation that gold film remodeling does not occur in saturated vapor or for films immersed in liquid. With decreasing RH, the model predicts decreases in both the radii of curvature and the lateral area of the meniscus across which the capillary force acts. However, the capillary pressure increases with decreasing net meniscus curvature according to the Laplace equation.[55] In fact, the Lin−Meier model predicts that the (negative) capillary pressure increases faster than the contact area decreases, so the (attractive) capillary force increases as the RH decreases.

The trends seen in Figure 11 can account for our experimental observations of gold film remodeling in the presence of iodobenzene and water vapors. The N_2 carrier gas was saturated with iodobenzene or water at ambient temperature (approximately 20 °C). With respect to gold films held at elevated temperatures (60 °C), the gas stream is substantially subsaturated (RH < 100%) with respect to the condensable vapor. The psychrometric chart for water vapor in air[59] suggests that, at 60 °C, the relative humidity may be as low as 1%. Estimates of the vapor pressures of iodobenzene based on the Antione equation[60] give a similar RH value at 60 °C. Figure 11 shows that low RH values correspond to substantial capillary forces between neighboring gold particles. Hence, the model provides a plausible explanation for the mechanism by which condensable vapors lead to gold film remodeling in our experiments.

The low contact angle for iodobenzene on gold (0°) leads to a relatively large value of the capillary force—more than 5 times that estimated for water vapor at the same RH (contact angle 81°). This prediction is consistent with our observation that gold film remodeling occurs much more

(56) Overbury, S. H.; Bertrand, P. A.; Somorjai, G. A. *Chem. Rev.* **1975**, *75*, 547.
(57) Prado, M. O.; Fredericci, C.; Zanotto, E. D. *J. Non-Cryst. Solids* **2003**, *331*, 145.
(58) *CRC Handbook of Chemistry and Physics*, 60th ed.; CRC Press: Boca Raton, FL, 1983.
(59) Perry, R. H.; Chilton, C. H. *Chemical Engineers' Handbook*, 5th ed.; McGraw-Hill: New York, 1973.
(60) Reid, J. C.; Prausnitz, J. C.; Sherwood, T. K. *The Properties of Gases and Liquids*, 3rd ed.; McGraw-Hill: New York, 1977.

rapidly for exposure to iodobenzene vapor than water vapor. In general, for liquids with comparable values of $\gamma_{L,vap}$, the remodeling rate should scale inversely with $\cos(\theta_{L,Au})$.

The capillary force model may also explain the counterintuitive observation that the rate of gold film remodeling in house N_2 gas is much faster than that in water-laden N_2, but somewhat slower than that of N_2 carrying iodobenzene. As mentioned previously, capillary condensation of N_2 can be ruled out. However, contamination of the N_2 by low (ppm) levels of water, water ingress into the sample chamber, or repeated "loading" of water onto the film during exposure to the ambient atmosphere could lead to very low effective RH values and thus relatively high capillary forces (Figure 11). Pumping these films down to vacuum before reheating would remove the capillary water quickly; the evaporation time scale may be much faster than the characteristic time for the gold nanoparticle coalescence. Thus, ambient capillary water contamination might have little impact on film remodeling in a vacuum. In contrast, flowing N_2 over the films would dry them relatively slowly and would require passage through the low RH range where capillary forces would be greatest. Thus, slow removal of capillary water contamination from repeated exposure to ambient air could account for the remodeling seen in gold films exposed to nominally dry house N_2. We are currently testing these ideas through additional experiments in which we try to minimize exposure of the gold films to ambient humidity.

If the capillary force model is correct and our parameter estimates are reasonable, the capillary forces may become comparable to the yield shear strength of nonannealed bulk gold. We speculate that capillary forces not only draw together neighboring particles but also create significant stresses that accelerate "wet" sintering of the gold nanoparticles, leading to coalescence.

Conclusions

In this paper, we have reported a new method for remodeling the morphology of thin gold films deposited on glass slides. This method originated from a serendipitous observation that part of a thin gold film heated to 120 °C turned pink when exposed to styrene vapor. Although a previous group has noted and studied the effect of solvent evaporation on the morphology and optical properties of ultrathin silver and gold films, this is the first report of the explicit use of subsaturated condensable vapors for controlled remodeling of ultrathin metal films.

Vapor-assisted metal film remodeling is simple, reproducible, and versatile. We have used a variety of condensable vapors to remodel gold, silver, and chromium films on a variety of substrates in addition to glass. After the initial film is formed by metal evaporation and vapor deposition, vapor-assisted remodeling does not require high-vacuum processing, annealing at elevated temperatures, or surface contamination with other adsorbates. Metal film morphology can be controlled by the choice of the initial film thickness, exposure time, and substrate temperature. We have adapted a theoretical model for capillary condensation that we believe captures the essential elements of the vapor-assisted remodeling mechanism.

We are currently developing methods for continuous, in situ monitoring of the remodeling process using UV−vis−near-IR spectrophotometry, SEIRA, and SERS. The ability to readily tailor the morphology and optical properties of thin metal films will undoubtedly lead to more reproducible substrates for SERS and similar surface spectroscopic methods, with expected applications in chemical and biological sensing.

Acknowledgment. We acknowledge the U.S. Environmental Protection Agency (EPA/EPSCoR Grant R-82942401-0), NASA (Grant NLPN03-0404), and the National Science Foundation (Award CTS-0103135) for financial support of this work.

Supporting Information Available: Additional ESEM images, UV−vis spectra, and other results (as described in the text) (PDF). This material is available free of charge at http://pubs.acs.org.

CM051127W